

Article

Bonding Behavior and Mechanism of U(VI) by Chemically Modified *Deinococcus radiodurans*

Xiaoqin Nie ^{1,2,3,*}, Faqin Dong ^{1,3,*}, Mingxue Liu ³, Wencai Cheng ², Congcong Ding ², Liang Bian ³ 
and Shiyong Sun ³ 

- ¹ National Collaborative Innovation Center for Nuclear Waste and Environmental Safety, Southwest University of Science and Technology, Mianyang 621010, China
- ² Fundamental Science on Nuclear Wastes and Environmental Safety Laboratory, Southwest University of Science and Technology, Mianyang 621010, China; chwc712@163.com (W.C.); dingcongcong@swust.edu.cn (C.D.)
- ³ Key Laboratory of Solid Waste Treatment and Resource Recycle, Ministry of Education, Southwest University of Science and Technology, Mianyang 621010, China; liumingxue@swust.edu.cn (M.L.); bianliang@swust.edu.cn (L.B.); shysun@swust.edu.cn (S.S.)
- * Correspondence: niexiaoqin@swust.edu.cn (X.N.); fqdong@swust.edu.cn (F.D.)

Abstract: The goal of this study is to understand the role of various functional groups on the cell surface when the microorganisms are exposed to uranium (U(VI)). The biomass of *Deinococcus radiodurans* was subjected to chemical treatments to modify the carboxyl (-C=O), amino (-NH₂), phosphate (-PO₂⁻), and hydroxyl (-OH) groups, as well as the lipid fraction. The behavior and process of U(VI) biosorption by *Deinococcus radiodurans* were ascertained, followed by scanning electron microscopy (SEM) combined with energy disperse spectroscopy (EDS) and Fourier transform infrared spectroscopy (FTIR) analyses. Carboxyl esterification and amino methylation deteriorated the removal efficiency by 8.0% and 15.5%, respectively, while lipid extraction, phosphate esterification, and hydroxyl methylation improved the removal efficiency by 11.7%, 8.7%, and 4.1%, respectively. The kinetic results revealed that uranium biosorption behavior by the raw and chemically modified biomass fitted well with the model of pseudo-second-order kinetic ($R^2 = 0.9949\sim 0.9998$). FTIR and SEM-EDS indicated that uranium initially bound with the raw and chemically modified *Deinococcus radiodurans*, which was probably controlled by ion exchange at the first stage, followed by complexation with the -C=O and -NH₂ groups, which especially prefer to bond with P and O atoms on the -PO₂⁻ group.

Keywords: bonding; chemical modification; uranium; *Deinococcus radiodurans*



Citation: Nie, X.; Dong, F.; Liu, M.; Cheng, W.; Ding, C.; Bian, L.; Sun, S. Bonding Behavior and Mechanism of U(VI) by Chemically Modified *Deinococcus radiodurans*. *Minerals* **2021**, *11*, 1108. <https://doi.org/10.3390/min11101108>

Academic Editor: Eugen Andreiadis

Received: 7 September 2021

Accepted: 6 October 2021

Published: 9 October 2021

Publisher's Note: MDPI stays neutral with regard to jurisdictional claims in published maps and institutional affiliations.



Copyright: © 2021 by the authors. Licensee MDPI, Basel, Switzerland. This article is an open access article distributed under the terms and conditions of the Creative Commons Attribution (CC BY) license (<https://creativecommons.org/licenses/by/4.0/>).

1. Introduction

With the fast development of the nuclear industry, the treatment and remediation of the nuclear, especially uranium (U(VI)), waste environment are still a common concern [1–5]. A large amount of uranium-containing radioactive waste is generated from activities such as uranium mining, milling, extraction, fuel fabrication, reactor operation, spent fuel reprocessing, and its disposal [2–4]. Several investigators have reported the potential of living and dead biomass of microbial origin to remove uranium from solutions [6–11]. Bioremediation of uranium waste by microbes offers a good alternative to physiochemical methods in terms of in situ applicability and high removal efficiency at a rather low concentration of the metal ion [12]. The main processes that are currently employed in uranium bioremediation include enzymatic metal bioreduction of soluble U(VI) to sparingly soluble U(IV), adsorption on cell surface, biopolymers or dead biomass, and bioprecipitation of U(VI) with ligands like inorganic phosphate [7,11]. Indeed, most microorganisms are very sensitive to ionizing radiation, and their use for bioremediation in high radiation environments is limited [13]. Explorations into the possibility of using

Deinococcus radiodurans in high radiation environments also revealed the inherent organic solvent tolerance and metal reduction ability of this organism [14,15]. Previous studies have reported that the mechanisms of uranium on the bacterium (such as *Deinococcus radiodurans*)/wastewater interface mainly include bioreduction [16–19] and biomineralization [11,13]. Some researchers reported that uranium phosphate minerals that formed on the surface of the bacterium were the result of uranium biosorption by plenty of functional groups on the surface of cells such as $-C=O$, $-NH_2$, and $-OH$, followed by precipitation with organophosphorus and inorganic phosphorus released from the cell [20,21]. Liu et al. [2] reported the contribution of proteins and polysaccharides on the cell surface and detailed the interface interaction for biosorption of strontium ions by *Saccharomyces cerevisiae* under culture conditions, which was investigated through chemical modification, in addition to spectroscopic and mesoscopic methods. However, the interface progress and mechanism between the uranium and cell surface have not been clear until now, and there is especially still lack of knowledge on the mechanism of uranium interaction with surface groups on the cell surface of *Deinococcus radiodurans*.

In this paper, we focus on the role of functional groups on typical radiation-resistant bacterium, and the aims of this study are as follows: (1) to investigate the role and behavior of the main functional groups on the cell surface of *Deinococcus radiodurans* by chemical modification and batch experiment; and (2) to identify the mechanism of bonding between *Deinococcus radiodurans* and uranium via a combination of SEM-EDS, FTIR, NMR, HPLC, and XRD.

2. Materials and Methods

2.1. Material and Bacteria

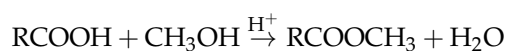
Uranium stock solution (1000 mg/L) was prepared by dissolving uranium nitrate [$UO_2(NO_3)_2 \cdot 6H_2O$] in 10 mL nitric acid and 990 mL distilled deionized water. Arsenazo III and other chemical reagents were of analytical grade. *Deinococcus radiodurans*, Gram-positive bacterium, was provided by the Experiment Center of Life Science and Engineering College in Southwest University of Science and Technology. The living bacteria were grown in 250 mL sterilized TGY broth culture medium, which contained tryptone (0.5%), yeast powder (0.3%), and glucose (1%) at $pH\ 7.0 \pm 0.1$ at $25 \pm 0.1\ ^\circ C$. The living *Deinococcus radiodurans* cells were harvested by centrifuging for 10 min at 4000 rpm and washed three times with deionized water. The raw biomass of *Deinococcus radiodurans* was prepared by putting living cells in the drying oven at $65\ ^\circ C$ for 24 h, and then the raw bacterial powder was collected as M0-raw biomass in this study.

2.2. Chemical Modifications of Biomass

Biomass was chemically modified in different ways in order to understand the role of functional groups in biosorption of uranium by the *Deinococcus radiodurans*. The chemical modifications were carried out as follows.

Extraction of lipid fraction [22]: 0.5 g raw biomass was contacted with 50 mL of acetone. The reaction mixture was shaken on a rotary shaker at 150 rpm for 6 h. The biomass residue obtained from this chemical treatment was referred to as M1.

Chemical modification of carboxyl group [23]: 0.5 g biomass was suspended in 25 mL anhydrous methanol, and 0.25 mL concentrated nitric acid was added to the suspension. The reaction mixture was shaken on a rotary shaker for 6 h at 150 rpm. The biomass residue obtained from this chemical treatment was referred to as M2. The general reaction took place as follows:



Chemical modification of amino group [23]: 0.5 g biomass was contacted with 10 mL formaldehyde (HCHO) and 20 mL formic acid (HCOOH). The reaction mixture was shaken

on a rotary shaker for 6 h at 150 rpm. The biomass residue obtained from this chemical treatment was referred to as M3. The general reaction took place as follows:



Chemical modification of phosphate group [23]: 0.5 g biomass was contacted with 20 mL triethyl phosphate and 15 mL of nitromethane. The reaction mixture was shaken on a rotary shaker for 6 h at 150 rpm. The biomass residue obtained from this chemical treatment was referred to as M4.

Chemical modification of hydroxyl group [24]: 0.5 g biomass was contacted with 10 mL formaldehyde (HCHO). The reaction mixture was shaken on a rotary shaker for 6 h at 150 rpm. The biomass residue obtained from this chemical treatment was referred to as M5.

The resulting biomass was collected by centrifugation at 4000 rpm for 10 min, washed three times with deionized water, and dried at 65 °C for 24 h.

2.3. Batch Experiment

All bonding experiments were conducted at biomass concentration of 0.25 g/L in a 500 mL conical flask containing 200 mL of 50 mg/L uranium solutions at pH 5 on a rotary shaker with 150 rpm at 35 °C, which was standardized as the optimum conditions in our preliminary studies [9]. This study focused on the migration of uranium tailing contamination. Considering the slightly acidic environment in uranium tailing and the best bonding behavior at this condition, pH 5.0 was chosen. The initial pH of the solution was adjusted with 0.01 mol/L HCl or 0.05 mol/L Na₂CO₃ solution. After shaking the flasks for different times from 5 min to 24 h, the reaction mixture was subjected to centrifugation at 4000 rpm for 10 min to obtain the suspensions. The concentrations of U(VI) in the initial and supernatant were determined with UV/vis spectrophotometer (at a wavelength of 652 nm) by Arsenazo (III) calorimetry. The percentage removal efficiency (*R*%) and the biosorption capacity per unit weight of adsorbent *q_t* (mg/g) at time *t* (min) were calculated according to Equations (1) and (2):

$$R\% = \frac{C_0 - C_t}{C_0} \times 100\% \quad (1)$$

$$q_t = \frac{(C_0 - C_t)V}{m} \quad (2)$$

where *C₀* (mg/L) and *C_t* (mg/L) were the solution concentration of U(VI) at the start and time *t*, respectively. *V* (L) was the volume of the solution and *m* (g) was the weight of the used adsorbent, and *q_t* (mg/g) was the adsorption capacity at time *t*. All experiment data were performed in triplicate, shown as the means.

2.4. Characterization of U-Loaded and Unloaded Samples

SEM-EDS was examined on ZEISS Ultra55 field emission scanning electron microscope coupled with Oxford IE450X-Max80 energy dispersive spectrometer. After air drying and gold-sputtering for 150 s, samples were analyzed using a high-resolution SEM instrument. For EDS analysis, the electron beam was ejected vertically in the horizontal placement of sample plane at an accelerating voltage of 15 keV and magnification of 9000 times. Fourier transform infrared spectra (FTIR) were collected from a Perkin-Elmer Nicolet-5700 spectrophotometer in the wavenumber range of 400–4000 cm⁻¹ at 25 °C. Bacteria before and after U(VI) biosorption by raw biomass and modified biomass as a function of active functional groups on the bacteria were obtained for FTIR analysis after mixing 2 mg biomass in 200 mg of KBr in order to prepare translucent sample disks. Bacteria before and after U(VI) biosorption by of modified phosphate group biomass were obtained for 1H nuclear magnetic resonance analysis (NMR, Advance III 600MHz, Bruker, Switzerland), high performance liquid chromatography (HPLC, NU3001D, Hanbang, huaian, China) analysis, and X-ray diffraction (XRD) patterns (D8Advance, Bruker, Germany).

2.5. Biosorption Kinetics

In order to obtain more useful information to confirm the underlying mechanisms during the entire removal process, a few kinetic models have been employed to describe the adsorption kinetics. Among these models, pseudo-first-order model and pseudo-second-order model and intraparticle diffusion kinetics model are mostly used to describe the adsorption kinetics. The nonlinear pseudo-first-order model [25] is expressed as follows (Equation (3)):

$$q_t = q_e \left(1 - e^{-k_1 \cdot t}\right) \quad (3)$$

where q_e and q_t are the adsorption capacity per unit weight of adsorbent (mg/g) at equilibrium and at time t (min), respectively, and k_1 is the pseudo-first-order rate constant (min^{-1}).

The linear form of the pseudo-second-order equation [26] is expressed as Equation (4):

$$\frac{t}{q_t} = \frac{1}{k_2 q_e^2} + \frac{t}{q_e} \quad (4)$$

$$h = k_2 q_e^2 \quad (5)$$

where k_2 is the pseudo-second-order rate constant ($\text{g} \cdot \text{mg}^{-1} \cdot \text{min}^{-1}$). The values of t/q_t are plotted against t , and the predicted adsorption capacity q_e ($\text{mg} \cdot \text{g}^{-1}$) and k_2 are calculated from the slope and intercept of the plot, respectively, and h [$\text{mg}/(\text{g} \cdot \text{min})$] is the pseudo-second-order initial rate constant.

The linear form of the intraparticle diffusion kinetics equation [27] is expressed as Equation (6):

$$q_t = k_3 t^{0.5} + C \quad (6)$$

where k_3 is the intraparticle diffusion kinetics rate constant ($\text{g} \cdot \text{mg}^{-1} \cdot \text{min}^{-0.5}$).

3. Results

3.1. SEM Observations of the Raw and Chemically Modified Biomass

The morphology of raw cells (Figure 1a) was complete, and the four dimeric structure of the independent cells was clear. However, the chemically modified cells were destroyed seriously in comparison with the raw ones. Accordingly, only a few bacteria could maintain the complete cell shape. In particular, the four dimeric structures of chemically modified cells disappeared, and the cells were transferred into sphericity or adhesion lumps.

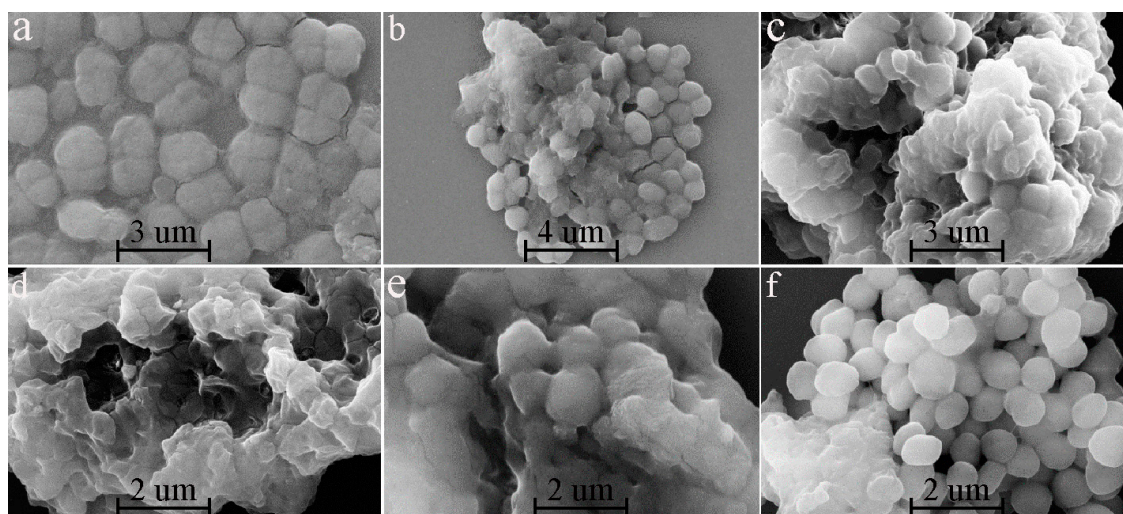


Figure 1. SEM micrographs of the raw and chemically modified biomass. (a) Unmodified biomass. (b) Extraction of lipid fraction. (c) Modification of amino group. (d) Modification of carboxyl group. (e) Modification of phosphate group. (f) Modification of hydroxyl group.

3.2. Changes in the Functional Groups of Chemically Modified *D. radiodurans*

The changes in the functional groups between the raw and chemically modified biomass were confirmed by FTIR spectroscopy. The bacterial envelope appears to be organized in different complexes of high molecular weight, mainly owing to its complex S-layer [28]. S-layer is organized in a repetition of the elementary components characterized by an internal sixfold symmetry [29,30]. In addition, although the *D. radiodurans* is a gram positive bacterium stain, the cell wall includes an outer membrane-like that represents a vestigial reminiscence of gram-negative ancestors [31,32]. The major cell wall components include proteins, lipid, carbohydrates, and carotenoids [33].

The corresponding infrared adsorption frequencies are illustrated in Figure 2 and Table 1. M1 represented the biomass of lipid extracted. The amide I band shifted from 1658 to 1654 cm^{-1} . Spectral analysis also revealed a reduction in the adsorption peak at 1658 and 1069 cm^{-1} in comparison with the raw biomass. M2 represented the biomass of carboxyl esterification, which exhibited the apparent shift of C-O stretching of COOH from 1395 to 1375 cm^{-1} . It showed that a significant change in the carboxyl group was presented in the biomass. The treatment resulted in the peak at 1625 cm^{-1} , which was indicative of the presence of formic acid [19]. M3 was attributed to the biomass of amino methylation. The peaks at 3628, 1544, and 1231 cm^{-1} in the biomass were reduced and broadened. It also indicated the enhancement of the band at 1453 cm^{-1} , suggesting a drastic change of methyl. The investigators reported that hexamine and proteins belong to the major constituents of the cell wall, and the contributory role of amino groups in Cr binding could be assumed [22]. M4 represented the biomass of phosphate esterification. The peaks at 1069 and 1045 cm^{-1} were both reduced, which could be interpreted as the symmetrical stretching vibration of the phosphodiester group and the stretching peak of -C-O-P, respectively. However, there were also some other weak changes, exemplified by amide groups, carboxyl groups, and so on. M5 was attributed to the biomass of hydroxyl methylation. The peak belongs to the hydroxyl groups shifted from 3592 to 3625 cm^{-1} .

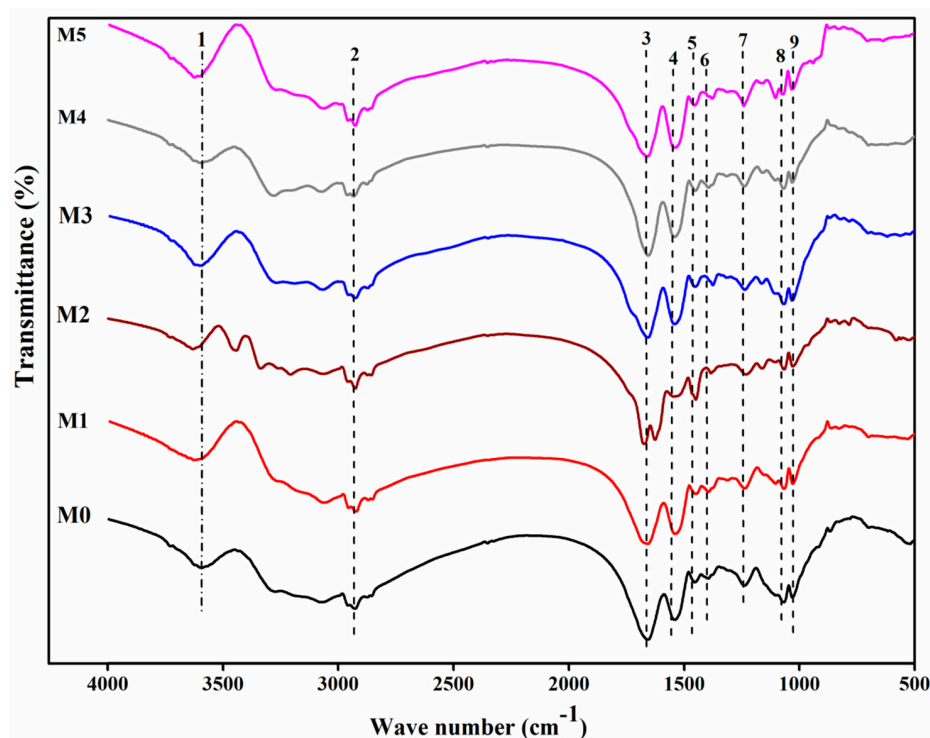


Figure 2. FTIR spectra of the raw and chemically modified *D. radiodurans*. M0, unmodified biomass. M1, extraction of lipid fraction. M2, modification of amino group. M3, modification of carboxyl group. M4, modification of phosphate group. M5, modification of hydroxyl group.

Table 1. Functional groups of the *D. radiodurans* and the corresponding infrared adsorption frequencies.

Number	Wave Number/cm ⁻¹	Assignment
1	3600	Hydroxyl groups of the glucose and the -NH stretching
2	2930	C-H stretching
3	1660	C=O stretching, amide I band of amide bond
4	1540	Amide II band
5	1450	Symmetric bending of CH ₃ of the acetyl moiety
6	1390	C-O stretching of COOH
7	1240	Amide III band, δO-H of COOH
8	1070	Phosphate group
9	1030	C-OH of carbohydrate
10	920	Asymmetric stretching vibration of ν_3 UO ₂ ²⁺ and stretching vibration of weakly bonded oxygen ligands with uranium (ν U-O _{ligand})

3.3. Removal Influenced by Time

Figure 3 shows the removal of raw and chemically modified biomass of *Deinococcus radiodurans* towards 50 mg/L U(VI) as a function of time. At the same time, the solution pH plays a vital role in the U(VI) removal process, as it affects not only the chemical properties and surface characteristics of biomass, the presence and distribution of U(VI) species in solution could be simulated by Visual MINEQL 3.0 (United States Environmental Protection Agency) [1,7], when pH at 5, uranium almost existed as uranyl cation and it is easy to combine with a negative charge on the surface of biomass. It was worth noting that biosorption follows as two processes. As previous studies [7–9] have shown that the first process was physical adsorption under the coulomb force, while the second process was metal coordination and ion exchange, which lead to the accumulation of U(VI) onto the biomass.

The biosorption of U(VI) by biomass both modified and unmodified was very rapid during the initial period and primarily occurred in the initial 3 h. In addition, the biosorption rate of biomass after lipid extraction and phosphate esterification was found to sharply increase and reach equilibrium in 3 h under the present experimental conditions. However, the biosorption by biomass after hydroxyl methylation reached equilibrium slowly, almost at the same time as the raw biomass, and the biosorption curve of biomass after carboxyl esterification was almost coincident with raw biomass. Although the biosorption process was too slow, such that it had not reached equilibrium in 24 h, the results (Figure 3) indicated that carboxyl esterification and amino methylation led to a removal rate decrease of 8.0% and 15.5%, respectively. The formaldehyde used for methylation of amino could also replace the H atoms present on -COOH. This could be attributed to the contribution of amino and carboxyl groups. While the removal rate of U(VI) was observed to be severely promoted when lipid was extracted, phosphate groups were esterified and hydroxyl groups were methylated. Furthermore, the removal rate was increased to 98.9%, 95.9%, and 91.4%, respectively. This could be attributed to the fact that the extraction with acetone removed the protein and lipid fraction of the biomass surface, which improved the biomass surface area of acetone-treated samples and exposed more metal binding sites [22].

Table 2 demonstrates that the potential biosorption capacity was similar with the raw biomass. Thus, the types of active site on the cell surface probably were just changed. It should also be noticed that the initial rate constants were promoted after chemical modification. Accordingly, the initial rate constant after lipid extraction was 16.7 times higher than the raw biomass. While the biosorption rate would decrease with time, followed by an equilibrium process as the secondary period.

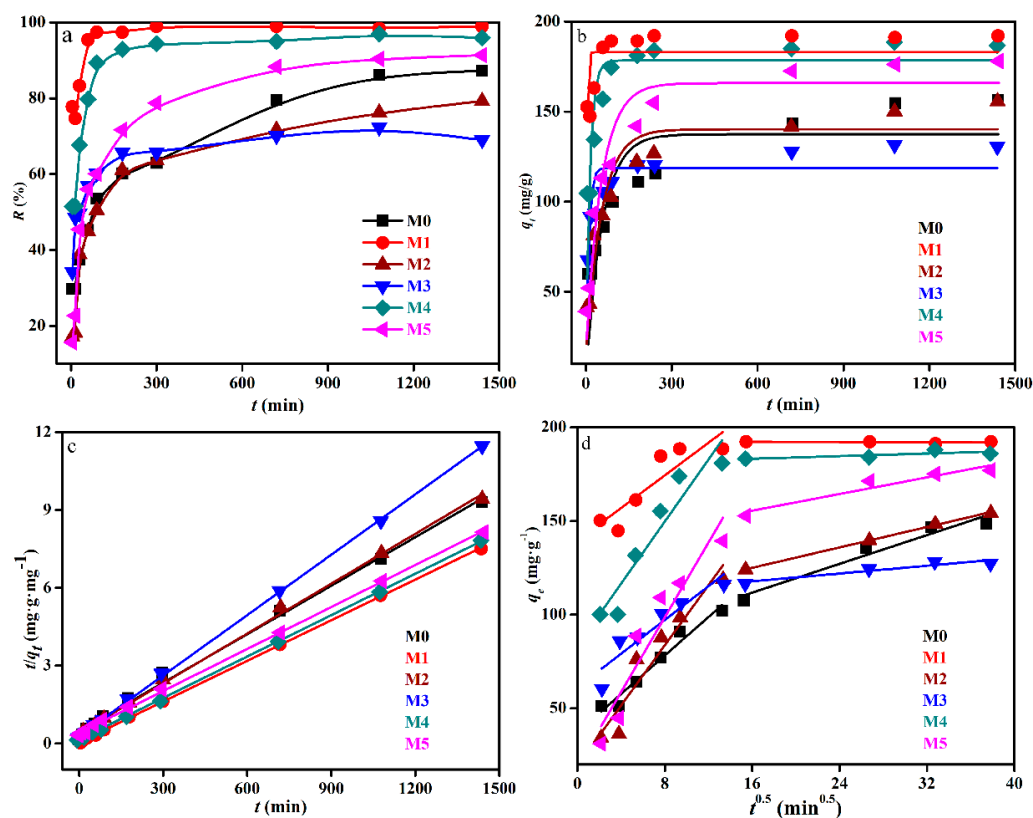


Figure 3. Uranium biosorption efficiency by the raw and chemically modified biomass of *Deinococcus radiodurans* (a), simulation of kinetics data of the raw and chemically modified biomass of *Deinococcus radiodurans* by the pseudo-first-order-model (b), pseudo-second-order t model (c), and intraparticle diffusion model (d). M0, unmodified biomass. M1, extraction of lipid. M2, modification of amino group. M3, modification of carboxyl group. M4, modification of phosphate group. M5, modification of hydroxyl group.

Table 2. Calculated pseudo-first-order and pseudo-second-order model coefficients.

Biomass	Pseudo-First-Order			Pseudo-Second-Order			Intraparticle Diffusion Kinetics			
	k_1 (min ⁻¹)	$q_{e(cal)}$ (mg/g)	R^2	$k_2 \times 10^{-3}$ (g/(mg·min))	$q_{e(cal)}$ (mg/g)	h (mg/(g·min))	R^2	k_3 (g/(mg·min ^{-0.5}))	C (mg/g)	R^2
M0	0.017	134.2	0.6491	1.08	159.0	2.60	0.9949	2.95	55.2	0.9263
M1	0.323	182.1	0.2203	18.77	191.6	43.46	0.9998	1.01	162.7	0.4032
M2	0.018	137.2	0.8897	1.28	155.5	3.14	0.9982	3.06	53.4	0.7760
M3	0.103	114.3	0.6397	4.95	127.7	8.29	0.9997	1.44	82.7	0.6710
M4	0.066	177.0	0.6225	5.52	186.9	19.21	0.9998	2.10	125.1	0.5197
M5	0.018	164.1	0.9253	1.27	182.1	4.01	0.9993	3.64	63.4	0.7323

The relative data were tabulated in Table 2. For many adsorption systems, the pseudo-first-order model was found to fit the experimental data for an early stage of adsorption ($R^2 = 0.2203\sim 0.9253$), and gradually deviated from the fitted curve along with the adsorption [34]. As shown in Table 2, pseudo-second-order kinetics equation data were found to fit to the model very well in the whole range of the metal–biomass interaction time. The values of q_e obtained from these plots correlated well with the values measured experimentally with strong correlation ($R^2 = 0.9949\sim 0.9998$).

3.4. Characterization of the Surface Properties Change after U(VI) Biosorption

Figure 4 shows the FTIR spectrum of raw biomass and the modification after biosorption of uranium. M1 showed the FTIR spectrum of biomass of lipid extracted after exposure to uranium. The peak shifted from 1396 to 1376 cm^{-1} . Moreover, the peak at 1237 cm^{-1} almost disappeared. These shifts could be attributed to the fact that carboxyl and amino

groups were involved in biosorption. Chen et al. [35] reported that the biomass of lipid extracted could expose more metal binding sites and improve the adsorptive property of the biomass. These sites could be interpreted as being because of carboxyl and amino groups. The appearance of a new peak at 918.6 cm^{-1} and changes in peak positions and intensity around the $550\text{--}1000\text{ cm}^{-1}$ region could be assigned to asymmetric stretching vibration of $\nu_3\text{ UO}_2^{2+}$ and stretching vibration of weakly bonded oxygen ligands with uranium ($\nu\text{ U-O}_{\text{ligand}}$) [36,37]. M2 showed the FTIR spectrum of biomass of carboxyl esterification after exposure to uranium. Compared with the biosorption of raw biomass, there was only an exceptionally slightly change at 1236 cm^{-1} . The shift from 1657 to 1660 cm^{-1} and the shift from 1541 to 1536 cm^{-1} indicated that the carboxyl group was not involved in biosorption and amino groups were one of the important functional groups in the biosorption of biomass of carboxyl esterification. Moreover, a new peak at 917 cm^{-1} could also be found. M3 showed the FTIR spectrum of biomass of amino methylation after exposure to uranium. Although amino methylation deteriorated the removal efficiency decrease 15.5% in comparison with the raw biosorption, the peak at 1672 cm^{-1} also shifted 12 cm^{-1} after modification. This could be primarily because of the heavy biosorption of amino on C-N. The investigators reported that nitrogen and oxygen atoms in the amide of cells would interact with U(VI) by a complex mechanism, including coordination, complexation, and so on. Therefore, electron cloud density of C-N, C-O, N-H, and other organic bonds was reduced, and the vibration frequency was changed. Moreover, the lone pair electrons of nitrogen atoms on the amino could also form coordination bonds with UO_2^{2+} . In addition, the peak at 1625 cm^{-1} disappeared after the biosorption, which suggested that remaining methyl was not taken out. M4 showed the FTIR spectrum of biomass of phosphate esterification after exposure to uranium. Compared with the primary groups as amide groups, the phosphate group shifted slightly at 1068 cm^{-1} . The biomass of phosphate esterification had just a slight change in comparison with the disappearance of raw biomass after biosorption. However, phosphate esterification improved the removal efficiency by 8.7%. In light of these facts, it could be interpreted as being because the ester group has a more significant effect on the biosorption than the phosphate group. Moreover, a new peak at 917 cm^{-1} could be found. M5 showed the FTIR spectrum of biomass of hydroxyl methylation after exposure to uranium. The peaks at 3625 and 1028 cm^{-1} in the biomass were increased in intensity. It is unclear whether the hydroxyl groups were methylated because almost all peaks were dangling free and did not have an apparent change. Therefore, we cannot find the primary group in the biosorption of biomass of hydroxyl methylation.

3.5. SEM-EDS and Spectroscopy Results of the Biomass after Uranium Biosorption

SEM confirmed the existence of distinct bioprecipitation of uranium on the surface of the raw biomass. Further SEM observations indicated the formation of needle-like crystals after exposure to the U(VI) solution (Figure 5a), while no similar bioprecipitation of uranium on the surface of biomass modification of the phosphate group took place (Figure 5b). After biosorption of *Deinococcus radiodurans*, both treated and untreated, the content of P was increased. This could be because the enzyme resides in periplasm and cleaves a phosphomonoester to release inorganic phosphate from the inside of cells and generate a high, local concentration of inorganic phosphate, which could precipitate uranium. The chemical nature of the precipitate was revealed by powder X-ray diffraction (XRD) studies to be uranyl hydrogen phosphate (HUO_2PO_4) [7,11]. However, there was no evidence to suggest that the crystals formed on the surface of the modified biomass in this study (Figure 6c).

NMR and HPLC can help us better understand the interaction between uranium and biomass. From Figure 6, we could preliminary find that the hydrogen spectrum of nuclear magnetism changes obviously in displacement and intensity, except for the water peak (between 3 and 4 ppm) and the solvent peak of tetramethylsilane (near 0 ppm). During scanning by HPLC, the obvious peak that appeared at near 3 min had its intensity

weakened after M4 reaction with uranium, and it is hard to make sure of the specific chemical substances in this study; it was probably caused by the chemically modified reagent of triethyl phosphate and nitromethane.

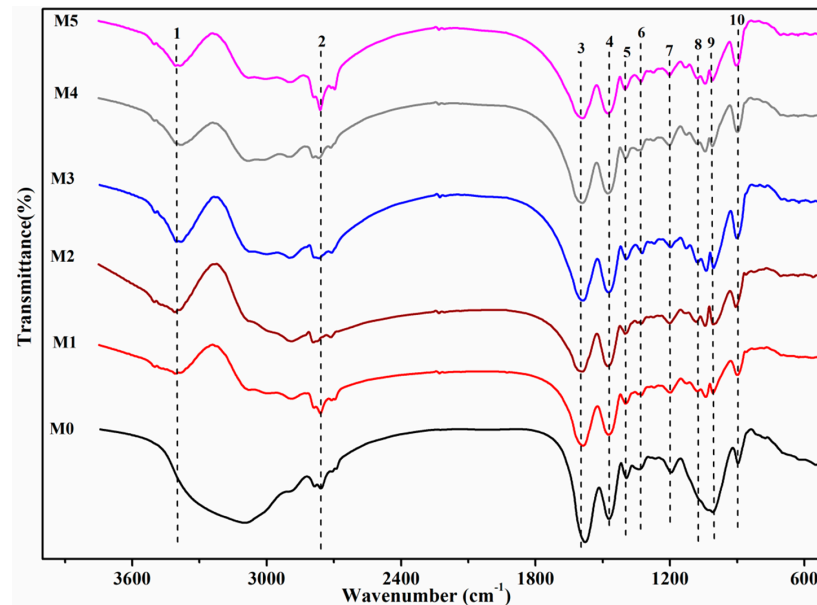


Figure 4. FTIR spectra of the raw and modified *Deinococcus radiodurans* after biosorption of uranium ($C_0 U(VI) = 50 \text{ mg}\cdot\text{L}^{-1}$ (dry biomass) = $0.25 \text{ g}\cdot\text{L}^{-1}$, pH = 5.0, temperature = 35°C , $t = 3 \text{ h}$). M0, unmodified biomass. M1, extraction of lipid fraction. M2, modification of amino group. M3, modification of carboxyl group. M4, modification of phosphate group. M5, modification of hydroxyl group.

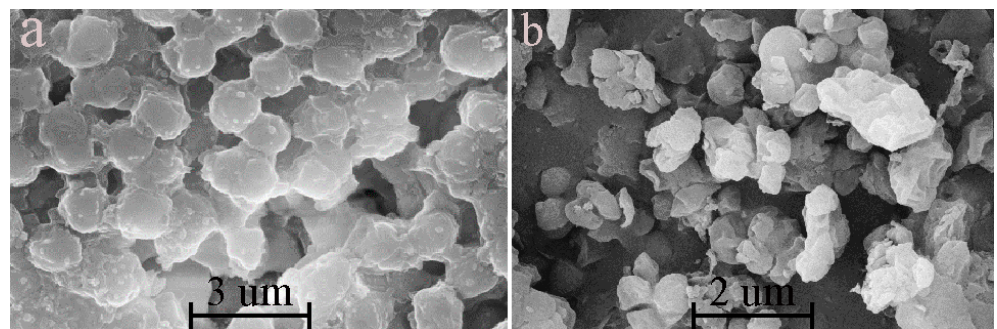


Figure 5. SEM micrographs of the biomass of *Deinococcus radiodurans* after biosorption of uranium. (a) unmodified biomass. (b) modification of the phosphate group.

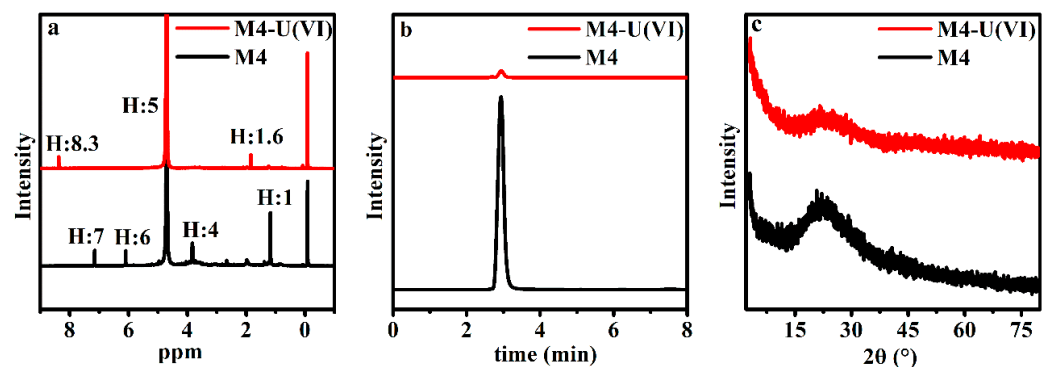


Figure 6. NMR (a), HPLC (b), and XRD (c) of the biomass of *Deinococcus radiodurans* of M4 (phosphate esterification) before and after biosorption of uranium.

4. Discussion

4.1. Microscopy and Spectroscopy Observations of the Raw and Chemically Modified Biomass

The problem that chemically modified cells were seriously destroyed arose in part from the concentration of organic reagents, which meant that cell membrane was dissolved with organic reagents, and the structure was damaged. In addition, the decomposition products of cells could further react with uranium. In light of this fact, the influence of adsorption capacity by modification could be interpreted as threefold: (1) transformation of cell surface groups; (2) change of the specific surface area [22]; and (3) the disintegration products of cells [38–42]. SEM (Figure 5) showed that uranium did not cause obvious damage to raw biomass of *Deinococcus radiodurans* and after phosphate esterification. This is consistent with the toxic effects of strontium on cells [2]. There were some dotted irregular uranium-bearing deposits on the surface of raw biomass, but no similar deposits on the surface of chemical modification biomass (Figure 5). It is inferred that mineralization is inhibited. EDS (Figure 7) showed that different from the raw biomass, the biosorption of biomass of phosphate esterification led to the drastic decrease of Na, K, and Mg ions, which suggested that biosorption was similar to metal removal by ion-exchange. Therefore, we could find that the primary mechanism of the raw biomass and modified biomass with U(VI) was different.

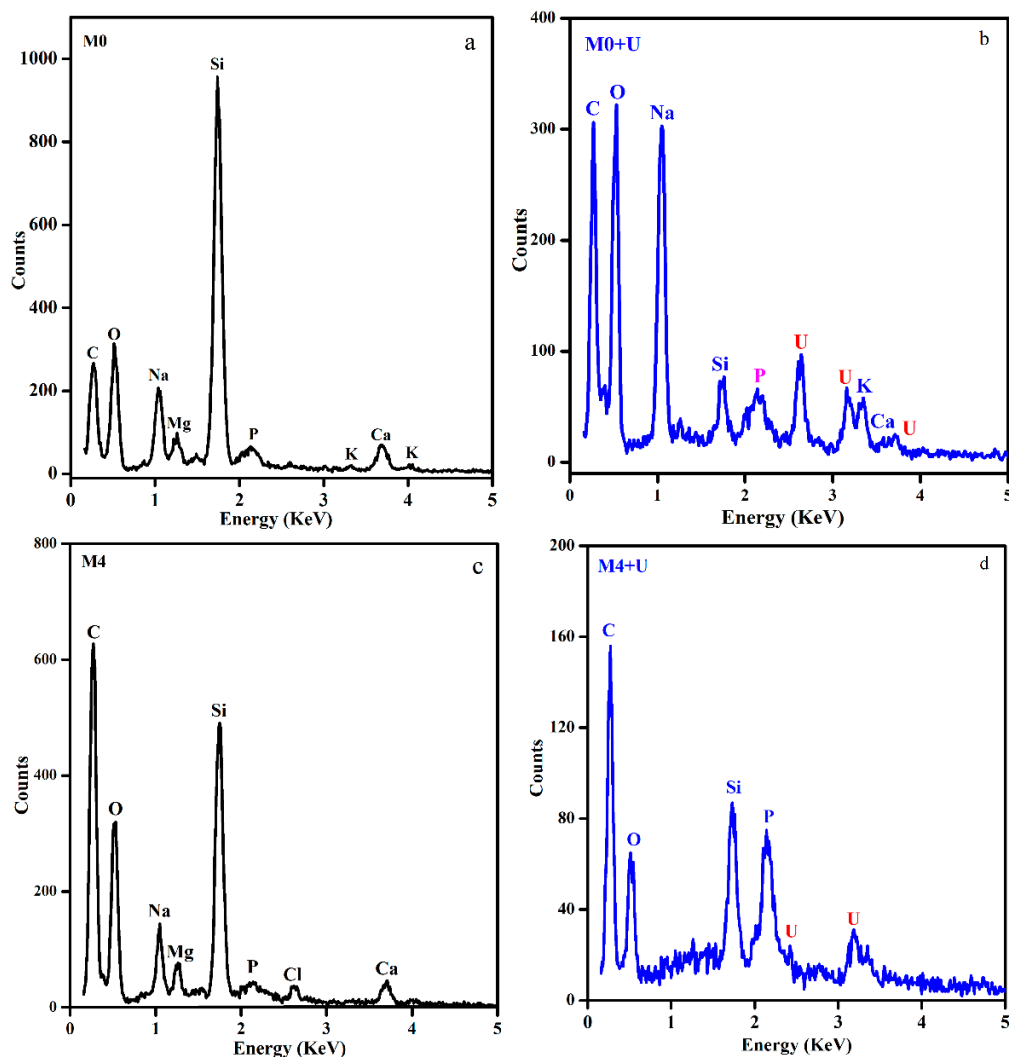


Figure 7. EDS micrographs of the biomass of *Deinococcus radiodurans* before and after biosorption of uranium. (a) Unmodified biomass before adsorption. (b) Unmodified biomass after biosorption. (c) Biomass of phosphate esterification. (d) Biomass of phosphate esterification after biosorption.

It should be noted that chemical modification could not have an accurate effect on the specific group. However, the result of FTIR demonstrated that it almost shielded all the specific groups. Therefore, all the tests in the following investigations could suggest that the consequences were mainly caused by the modification of relevant functional groups. Overall, FTIR spectra analysis implied that carboxyl and amino groups play the primary role during the interaction of biomass and uranium. Moreover, the new peak of uranium at 917 cm^{-1} could always be found after biosorption. According to the expert suggestion, we tried to measure the NMR and HPLC on the biomass of *Deinococcus radiodurans* by phosphate esterification before and after reaction with uranium. The results of the preliminary analysis showed that hydrogen functional groups such as the amino group, carboxyl group, and modified reagent all played an obvious role in the M4 biomass biosorption of uranium.

4.2. Uranium Removal Influenced by Time

It could be speculated that the surface active sites were fully occupied and reached saturation in the process of surface biosorption. At the same time, the precipitation of U-phosphate probably occurred on cell surfaces during the equilibrium process [41]. Moreover, uranium could also be transferred to the internal surroundings of cells. Finally, it should be noted that there has been a different change trend by the biomass of lipid extracted and amino methylation; the raw and other chemically modified biomass could still work after the initial period. To a certain extent, five functional groups would affect the process of biosorption. Overall, the carboxyl group and amino group played the primary role in the process.

As previous research mentioned, Park, D. et al. [43] reported that hat acetone treatment could enhance the removal efficiency of total Cr from 60% to 86%, and they suggested that the biomass of lipid extracted could expose more metal binding sites and improve the adsorptive property of the biomass. Chen et al. [35] demonstrated that formaldehyde treatment significantly enhanced the removal efficiency of Cu(II), Pb(II), and Ni(II) for the prevention of organic leaching. Yang et al. [38] reported that hat formaldehyde treatment significantly enhanced the removal efficiency of Cr(VI). In addition, the contribution of the amino group would further depend on the extent of its protonation at pH 5.0. Figure 4 indicates that the biosorption was more sensitive to the amino methylation than the others.

The actual biosorption capacity fitted well with the pseudo-second-order kinetics model, which suggested that pseudo-second-order kinetics could represent all the processes of biosorption in this study, which include the physical adsorption process and chemical bonding process. Therefore, pseudo-second-order kinetics could better represent the biosorption mechanism. In addition, rate constant (k_2) and initial rate constant (h) were found to be promoted after all kinds of modifications, which meant it became easier for them to reach equilibrium than the raw biomass.

5. Conclusions

This study on biomass modification for the elucidation of the U(VI) binding mechanism suggested that the methods of modification could almost shield all the specific functional groups. All the investigations suggest that the consequences were caused by the modification of relevant groups. Carboxyl esterification and amino methylation led to uranium removal efficiency decrease of 8.0% and 15.5%, respectively. On the contrary, modifications of lipid, phosphate, and hydroxyl could improve the uranium removal efficiency from 87.2% to 98.9%, 95.9%, and 91.4%, respectively. The experimental results of this study demonstrated that carboxyl ($-\text{C}=\text{O}$) and amino ($-\text{NH}_2$) groups could be the main binding sites on the biomass surface for *Deinococcus radiodurans* biosorption. Moreover, it should be noted that the surface feature of modified biomass was apparently changed after modification, which probably meant that the electric potential was changed so that uranium was rapidly adsorbed under the coulomb force. In addition, pseudo-second-order kinetics equation data fitted well in the whole range of the metal–biomass interaction time,

as the values of q_e obtained from these plots correlated well with the values measured experimentally with a strong correlation ($R^2 = 0.9949\sim 0.9998$). SEM-EDS results suggested that the released P from the inside of cells reacted with adsorbed U(VI) on the cell surfaces of raw biomass, resulting in the formation of U(VI) precipitates, even though no P was added to the exposure solution. The P and O atoms of the $-\text{PO}_2^-$ group could coordinate with uranium ions during the U(VI) biosorption.

Author Contributions: All authors contributed to this manuscript. F.D. and M.L. conceived and designed the study. X.N., C.D. and W.C. performed the experiments. X.N. performed the data analysis and wrote this manuscript. L.B. and S.S. guided the structure and contents of the paper and improved earlier drafts. All authors have read and agreed to the published version of the manuscript.

Funding: This research was funded by National Natural Science Foundation of China, grant number 41877323.

Acknowledgments: We are very grateful to Jialin Ma and Huiping Tang for their help in the experiment and drawing of the figures.

Conflicts of Interest: The authors declare no conflict of interest.

References

- Nie, X.; Dong, F.; Bian, L.; Liu, M.; Ding, C.; He, H.; Yang, G.; Sun, S.; Qin, Y.; Huang, R. Uranium binding on *Landoltia punctata* as a result of formation of insoluble nano-U(VI) and U (IV) phosphate minerals. *ACS Sustain. Chem. Eng.* **2017**, *5*, 1494–1502. [[CrossRef](#)]
- Liu, M.; Dong, F.; Zhang, W.; Nie, X.; Wei, H.; Sun, S.; Zhong, X.; Liu, Y.; Wang, D. Contribution of surface functional groups and interface interaction to biosorption of strontium ions by *Saccharomyces cerevisiae* under culture conditions. *RSC Adv.* **2017**, *7*, 50880–50888. [[CrossRef](#)]
- Sanchez-Castro, I.; Martinez-Rodriguez, P.; Jroundi, F.; Solari, P.L.; Descostes, M.; Merroun, M.L. High-efficient microbial immobilization of solvated U(VI) by the *Stenotrophomonas* strain Br 8. *Water Res.* **2020**, *183*, 116110. [[CrossRef](#)]
- Wang, Y.; Frutschi, M.; Suvorova, E.; Phrommavanh, V.; Descostes, M.; Osman, A.A.A.; Geipel, G.; Bernier-Latmani, R. Mobile uranium(IV)-bearing colloids in a mining-impacted wetland. *Nat. Commun.* **2013**, *4*, 2942–2947. [[CrossRef](#)] [[PubMed](#)]
- Suzuki, Y.; Kelly, S.; Kemner, K.; Banfield, J.F. Nanometre-size products of uranium bioreduction. *Nature* **2002**, *419*, 134. [[CrossRef](#)]
- Tang, H.; Cheng, W.; Yi, Y.; Ding, C.; Nie, X. Nano zero valent iron encapsulated in graphene oxide for reducing uranium. *Chemosphere* **2021**, *278*, 130229. [[CrossRef](#)] [[PubMed](#)]
- Kulkarni, S.; Ballal, A.; Apte, S.K. Bioprecipitation of uranium from alkaline waste solutions using recombinant *Deinococcus radiodurans*. *J. Hazard. Mater.* **2013**, *262*, 853–861. [[CrossRef](#)] [[PubMed](#)]
- Pang, C.; Liu, Y.H.; Cao, X.H.; Li, M.; Huang, G.-L.; Hua, R.; Wang, C.-X.; Liu, Y.-T.; An, X.-F. Biosorption of uranium (VI) from aqueous solution by dead fungal biomass of *Penicillium citrinum*. *Chem. Eng. J.* **2011**, *170*, 1–6. [[CrossRef](#)]
- Daboor, S.M. Application of bacterial biomass as a potential heavy metal bio-removal agent. *Afr. J. Microbiol. Res.* **2014**, *8*, 2229–2237.
- Nie, X.; Dong, F.; Liu, N.; Liu, M.; Zhang, D.; Kang, W.; Sun, S.; Zhang, W.; Yang, J. Subcellular distribution of uranium in the roots of *Spirodela punctata* and surface interactions. *Appl. Surf. Sci.* **2015**, *347*, 122–130. [[CrossRef](#)]
- Huang, W.; Nie, X.; Ding, C.; Huang, R.; Dong, F.; Sun, S.; Qin, Y.; Liu, M. Kinetics and pH-dependent uranium bioprecipitation by *Shewanella putrefaciens* under aerobic conditions. *J. Radioanal. Nucl. Chem.* **2017**, *312*, 531–541. [[CrossRef](#)]
- Alessi, D.S.; Lezama-Pacheco, J.S.; Stubbs, J.E.; Janousch, M.; Bargar, J.R.; Persson, P.; Bernier-Latmani, R. The product of microbial uranium reduction includes multiple species with U (IV)–phosphate coordination. *Geochim. Cosmochim. Acta* **2014**, *131*, 115–127. [[CrossRef](#)]
- Nie, X.; Dong, F.; Liu, M.; He, H.; Sun, S.; Bian, L.; Yang, G.; Zhang, W.; Qin, Y.; Huang, R. Microbially mediated stable uranium phosphate nano-biomaterials. *J. Nanosci. Nanotechnol.* **2017**, *17*, 6771–6780. [[CrossRef](#)]
- Lange, C.C.; Wackett, L.P.; Minton, K.W.; Daly, M.J. Engineering a recombinant *Deinococcus radiodurans* for organopollutant degradation in radioactive mixed waste environments. *Nat. Biotechnol.* **1998**, *16*, 929–933. [[CrossRef](#)] [[PubMed](#)]
- Fredrickson, J.K.; Kostandarithes, H.M.; Li, S.W.; Plymale, A.E.; Daly, M.J. Reduction of Fe (III), Cr (VI), U(VI), and Tc (VII) by *Deinococcus radiodurans* R1. *Appl. Environ. Microbiol.* **2000**, *66*, 2006–2011. [[CrossRef](#)] [[PubMed](#)]
- Bernier-Latmani, R.; Veeramani, H.; Vecchia, E.D.; Junier, P.; Lezama-Pacheco, J.S.; Suvorova, E.I.; Sharp, J.O.; Wigginton, N.S.; Bargar, J.R. Non-uraninite products of microbial U(VI) reduction. *Environ. Sci. Technol.* **2010**, *44*, 9456–9462. [[CrossRef](#)] [[PubMed](#)]
- Plathe, K.L.; Lee, S.W.; Tebo, B.M.; Bargar, J.R.; Bernier-Latmani, R. Impact of microbial Mn oxidation on the remobilization of bio-reduced U (IV). *Environ. Sci. Technol.* **2013**, *47*, 3606–3613. [[CrossRef](#)] [[PubMed](#)]
- Stylo, M.; Alessi, D.S.; Shao, P.P.Y.; Lezama-Pacheco, J.S.; Bargar, J.R.; Bernier-Latmani, R. Biogeochemical controls on the product of microbial U(VI) reduction. *Environ. Sci. Technol.* **2013**, *47*, 12351–12358. [[CrossRef](#)]

19. Stylo, M.; Neubert, N.; Roebbert, Y.; Weyer, S.; Bernier-Latmani, R. Mechanism of uranium reduction and immobilization in *Desulfovibrio vulgaris* biofilms. *Environ. Sci. Technol.* **2015**, *49*, 10553–10561. [[CrossRef](#)]
20. Choudhary, S.; Sar, P. Uranium biomineralization by a metal resistant *Pseudomonas aeruginosa* strain isolated from contaminated mine waste. *J. Hazard. Mater.* **2011**, *186*, 336–343. [[CrossRef](#)]
21. Liang, X.; Csetenyi, L.; Gadd, G.M. Uranium bioprecipitation mediated by yeasts utilizing organic phosphorus substrates *Appl. Microbiol. Biotechnol.* **2016**, *100*, 5141–5151. [[CrossRef](#)]
22. Bai, R.S.; Abraham, T.E. Studies on enhancement of Cr (VI) biosorption by chemically modified biomass of *Rhizopus nigricans*. *Water Res.* **2002**, *36*, 1224–1236. [[CrossRef](#)]
23. Kapoor, A.; Viraraghavan, T. Heavy metal biosorption sites in *Aspergillus niger*. *Bioresour. Technol.* **1997**, *61*, 221–227. [[CrossRef](#)]
24. Holan, Z.R.; Volesky, B. Accumulation of cadmium, lead, and nickel by fungal and wood biosorbents. *Appl. Biochem. Biotechnol.* **1995**, *53*, 133–146. [[CrossRef](#)]
25. Tran, H.N.; You, S.-J.; Hosseini-Bandegharai, A.; Chao, H.-P. Mistakes and inconsistencies regarding adsorption of contaminants from aqueous solutions: A critical review. *Water Res.* **2017**, *120*, 88–116. [[CrossRef](#)] [[PubMed](#)]
26. Zhuang, S.; Wang, J. Poly Amidoxime functionalized carbon nanotube as an efficient adsorbent for removal of uranium from aqueous solution. *J. Mol. Liq.* **2020**, *319*, 114288. [[CrossRef](#)]
27. Zhong, X.; Liang, W.; Lu, Z.; Qui, M.; Hu, B. Ultra-high capacity of graphene oxide conjugated covalent organic framework nanohybrid for U(VI) and Eu (III) adsorption removal. *J. Mol. Liq.* **2021**, *323*, 114603. [[CrossRef](#)]
28. Farci, D.; Bowler, M.W.; Kirkpatrick, J.; McSweeney, S.; Tramontano, E.; Piano, D. New features of the cell wall of the radio-resistant bacterium *Deinococcus radiodurans*. *Biochim. Biophys. Acta Biomembr.* **2014**, *183*, 1978–1984. [[CrossRef](#)]
29. Müller, D.J.; Baumeister, W.; Engel, A. Conformational change of the hexagonally packed intermediate layer of *Deinococcus radiodurans* monitored by atomic force microscopy. *J. Bacteriol. Res.* **1996**, *17*, 3025–3030. [[CrossRef](#)]
30. Baumeister, W.; Barth, M.; Hegerl, R.; Guckenberger, R.; Hahn, M.; Saxton, W.O. Three-dimensional structure of the regular surface layer (HPI layer) of *Deinococcus radiodurans*. *J. Mol. Biol.* **1986**, *18*, 241–250. [[CrossRef](#)]
31. Work, E. Chemical Structure of Bacterial Cell Walls: Amino-acids of Walls of *Micrococcus radiodurans*. *Nature* **1964**, *201*, 1107–1109. [[CrossRef](#)]
32. Knivett, V.A.; Cullen, J.; Jackson, M.J. Odd-numbered fatty acids in *Micrococcus radiodurans*. *Biochemistry* **1965**, *96*, 2C–3C. [[CrossRef](#)]
33. Rothfuss, H.; Lara, J.C.; Schmid, A.K.; Lidstrom, M.E. Involvement of the S-layer proteins Hpi and SlpA in the maintenance of cell envelope integrity in *Deinococcus radiodurans* R1. *Microbiology* **2006**, *152*, 2779–2787. [[CrossRef](#)]
34. Ho, Y.S.; McKay, G. Pseudo-second order model for sorption processes. *Process Biochem.* **1999**, *34*, 451–465. [[CrossRef](#)]
35. Chen, J.P.; Yang, L. Chemical modification of *Sargassum* sp. for prevention of organic leaching and enhancement of uptake during metal biosorption. *Ind. Eng. Chem. Res.* **2005**, *44*, 9931–9942.
36. Čejka, J. 12. Infrared Spectroscopy and Thermal Analysis of the Uranyl Minerals. In *Uranium*; De Gruyter: Berlin, Germany, 2018; pp. 521–622.
37. Li, X.; Ding, C.; Liao, J.; Lan, T. Biosorption of uranium on *Bacillus* sp. *dwc-2*: Preliminary investigation on mechanism. *J. Environ. Radioact.* **2014**, *135*, 6–12. [[CrossRef](#)]
38. Yang, L.; Chen, J.P. Biosorption of hexavalent chromium onto raw and chemically modified *Sargassum* sp. *Bioresour. Technol.* **2008**, *99*, 297–307. [[CrossRef](#)] [[PubMed](#)]
39. Nie, X.; Dong, F.; Liu, N. An investigation on the subcellular distribution and compartmentalization of uranium in *Phaseolus vulgaris* L. *J. Radioanal. Nucl. Chem.* **2014**, *299*, 1351–1357. [[CrossRef](#)]
40. Huang, G.; Ng, T.W.; An, T.; Li, G.; Xia, D.; Yip, H.Y.; Zao, Y.; Wong, P.K. Probing the intracellular organic matters released from the photocatalytic inactivation of bacteria using fractionation procedure and excitation-emission-matrix fluorescence. *Water Res.* **2017**, *110*, 270–280. [[CrossRef](#)] [[PubMed](#)]
41. Jiang, M.Y.; Ohnuki, T.; Tanaka, K.; Kozai, N.; Kamiishi, E.; Utsunomiya, S. Post-adsorption process of Yb phosphate nano-particle formation by *Saccharomyces cerevisiae*. *Geochim. Acta* **2012**, *93*, 30–46. [[CrossRef](#)]
42. Misra, C.S.; Appukuttan, D.; Kantamreddi, V.S.S.; Rao, S.A.; Apte, S.K. Recombinant *D. radiodurans* cells for bioremediation of heavy metals from acidic/neutral aqueous wastes. *Bioeng. Bugs* **2012**, *3*, 44–48. [[PubMed](#)]
43. Park, D.; Yun, Y.S.; Park, J.M. Studies on hexavalent chromium biosorption by chemically-treated biomass of *Ecklonia* sp. *Chemosphere* **2005**, *60*, 1356–1364. [[CrossRef](#)] [[PubMed](#)]